Impaired Functional Connectivity of Cortico-Amygdala Pathway Can Drive Social Behavior Deficits in Synucleinopathies

Wei Zhou[1,6], Samuel Daniels[1,2], Vijay Singh[4], Marissa Menard[4,5], Martha L Escobar Galvis[3], Hong-Yuan Chu[1,5,6*]

1 Department of Neurodegenerative Science, Van Andel Research Institute, Grand Rapids, MI 49503, USA

2 Van Andel Institute Graduate School, Grand Rapids, MI, 49503, USA

3 Core Technologies and Services Van Andel Institute, Grand Rapids, MI 49503, USA

4 Center for Neurodegeneration and Experimental Therapeutics, University of Alabama at Birmingham, Birmingham, Alabama 35294, USA

5 Aligning Science Across Parkinson's (ASAP) Collaborative Research Network, Chevy Chase, MD, 20852, United States

6 Department of Pharmacology and Physiology, Georgetown University Medical Center, Washington D.C., 20007, USA

*Corresponding author: Hong-Yuan Chu, Ph.D.; Email: hc948@georgetown.edu

Declarations

Ethics approval. Animal studies were reviewed and approved by the Institutional Animal Care and Use Committee at Van Andel Institute (animal use protocol #: 22-02-007) and in accordance with the standards of NIH for care and use of animals.

Availability of data and materials. The datasets used and/or analyzed during the current study have been deposited and are publicly available from the Open Science Framework (https://osf.io/p4zd5/?view_only=5d19bc80d7714c769cddcaccd7beb2c7).

Competing interests. The authors declare that they have no competing interests.

Funding. This work was partially supported by research grants from Brain and Behavior Research Foundation (grant#: 29037, H.Y.C.), Department of Defense Congressionally Directed Medical Research Programs (grant#: W81XWH-21-1-0943, H.Y.C.). This work was also funded in whole or in part by Aligning Science Across Parkinson's (ASAP-020572) through the Michael J. Fox Foundation for Parkinson's Research (MJFF) and Aligning Science Across Parkinson's Disease-PFF support and characterization (ASAP-022091) through the Michael J Fox Foundation for Parkinson's Research to LVD. For the purpose of open access, the authors have applied a CC BY public copyright license to all Author Accepted Manuscripts arising from this submission.

Authors' contributions. WZ conducted stereotaxic surgeries, electrophysiological recordings, and behavioral tests, analyzed data and interpreted results, and wrote initial draft. SD conducted stereotaxic surgeries and behavioral tests. VS and MM generated and validated mouse α-synuclein preformed fibrils and wrote the initial draft. MEG contributed to acquisition of grant supports, interpreting results, as well as writing and editing the manuscript. HYC contributed to conceptualization of the project, obtaining of grant supports and the

administration, as well as analyzing and interpreting data, writing, editing and revising the manuscript. All authors read and approved the final manuscript.

Author ORCIDs

Wei Zhou: 0009-0002-9069-4888

Samuel Daniels: 0000-0003-4985-3787

Vijay Singh: 0000-0002-5163-0876

Marissa Menard: 0000-0002-0976-3448

Martha L Escobar Galvis: 0000-0001-8400-9392

Hong-Yuan Chu: 0000-0003-0923-683X

Acknowledgement. Experimental work was conducted at Van Andel Research Institute. Data analysis was partially performed at Van Andel Research Institute and completed at Georgetown University Medical Center. The authors thank Van Andel Institute vivarium technician team for animal husbandry, and Ms. Rachel Dvorak for initial technical assistance in animal surgery. The authors thank Dr. Qiang Zhu at Van Andel Institute for general support in grant administration.

Abstract

The small molecule protein α-synuclein forms insoluble aggregates in a group of neurological disorders, including Parkinson's disease and dementia with Lewy bodies (DLB), which are collectively called synucleinopathies. In PD and DLB, the amygdala has been identified as a particularly susceptible region in the brain for the deposition of Lewy-like α-synuclein aggregates. Though α-synuclein aggregation is closely associated with neurodegeneration, there is a poor correlation between neurodegeneration in the amygdala and the clinical features of PD/DLB. We hypothesize that, prior to neurodegeneration, α-synuclein aggregation disrupts functional cortical modulation of the amygdala circuits, leading to emotion dysregulation in synucleinopathies. In the present study, we combined electrophysiology, optogenetics, mouse model of synucleinopathies, and behavioral analysis to test this hypothesis. Using an α-synuclein preformed fibrils (PFFs)-based mouse model of synucleinopathies, we reported dynamic changes in the levels of α-synuclein pathology in the basolateral amygdala (BLA). Such dynamic changes of pathology associated with a decreased cortico-BLA connection strength prior to a significant loss of cortical axon terminals. In parallel to the reduced cortico-BLA connection, PFFs-injected mice manifested impaired social preference behavior. The impaired sociability of PFFs-injected mice could be rescued by chemogenetic stimulation of cortico-BLA inputs. Altogether, we presented a series of evidence to delineate key circuit events associated with α-synuclein pathology development in the amygdala circuits. The present work highlights the necessity of a thorough investigation of functional consequences of α-synuclein aggregation to advance our understand of pathophysiology of synucleinopathies and development of effective therapies.

Keywords

α-synuclein, synucleinopathies, Parkinson's disease, medial prefrontal cortex, amygdala, electrophysiology, optogenetics, neural circuit, synapse, sociability

Background

Abnormally folded and aggregated α-synuclein (α-Syn) is the major proteinaceous component of the intraneuronal inclusions that characterize Lewy pathology [1, 2]. Lewy pathology can be found in most brains of people with Parkinson's disease (PD), dementia with Lewy bodies (DLB), and multiple system atrophy. These disorders are collectively known as "synucleinopathies" [2]. Experimental work suggests that gradual accumulation of α-Syn aggregates can underlie the pathogenesis and progression of synucleinopathies [3-5]. Particularly, accumulation of pathologic α-Syn aggregates has been reported to impair nigrostriatal dopaminergic neurotransmission and closely relate to the neurodegeneration, leading to the manifestation of motor symptoms in PD [4, 6, 7]. In addition, α-Syn pathology is proposed to spread between cells and brain regions [3, 5, 8, 9]. Consequently, a large body of studies have focused on understanding the genetic and microenvironmental factors that may promote or prevent the formation of pathologic α-Syn aggregation, as they perhaps can provide us with strategies to regulate the temporal development and spatial distribution of α-Syn pathology across brain regions and in that way modify disease progression [10-15].

Formation of α-Syn aggregates in the brain trigger series of circuitry events, including but not limited to, the degeneration of vulnerable neuronal populations. For example, compelling evidence also suggests that α-Syn aggregates disrupt synaptic structure, function, and plasticity in susceptible brain regions, like the nigrostriatal pathway [4, 16-18]. Motor dysfunction in PD is closely linked with dopamine depletion in the basal ganglia and the subsequent functional maladaptation within the basal ganglia-thalamocortical network [19, 20]. Similar pathophysiological processes are likely to occur in other brain regions that are

108 vulnerable to the formation of α-synuclein aggregates, in which functional circuit changes, not
109 necessarily neurodegeneration, are causally linked to symptom manifestation.
110 The amygdala has been reported as a preferential brain region for Lewy pathology
111 development in PD and DLB [21-24] and animal models of synucleinopathy [3, 25, 26].
112 Considering the critical role of the amygdala in emotion regulation, heavy load of Lewy-like
113 pathology in the amygdala and the subsequent neuronal loss are expected to causally associate
114 with depression and/or anxiety in PD/DLB [27-30].However, such a linear relationship between
115 neurodegeneration and clinical features has not been supported by studies using human tissues
116 of PD/DLB [24] or its animal models [25, 31]. Building on the research about the nigrostriatal
117 dopaminergic system, it is plausible to hypothesize that impaired amygdala circuit function, but
118 not significant neurodegeneration, is sufficient to cause emotion dysregulation in
119 synucleinopathies. In the present work, we combined electrophysiological,
120 immunohistochemical, and behavioral approaches to test this hypothesis. Using an intrastriatal
121 α-synuclein preformed fibrils (PFFs) model, we demonstrated that: 1) α-synuclein aggregates
122 selectively eliminate cortical afferents to the basolateral amygdala (BLA); 2) α-synuclein
123 aggregation induces functional impairment of cortico-BLA inputs, prior to robust synapse loss;
124 3) neuronal loss in the BLA occurs at late stages as α-synuclein aggregates accumulate; and 4)
125 social behavioral deficits associate with cortico-BLA synaptic impairments, occurring prior to
126 synaptic or neuronal loss in the BLA, and can be alleviated by functional restoration of cortico-
127 BLA connection strength. Our work here provides novel insights into the amygdala circuit
128 dysfunction associated with α-Syn pathology formation and possible biological mechanisms
129 underlying emotion dysregulation in PD and DLB.

130 **Materials and methods**

131 **Animals**

132 C57BL/6J mice at 2-3-month-old (Jax#:000664, RRID: IMSR_JAX:000664) of both sexes were
133 obtained through the Van Andel Institute vivarium and used in this study. All animal studies
134 were reviewed and approved by the Institutional Animal Care and Use Committee at Van Andel
135 Institute (animal use protocol #: 22-02-007) and in accordance with the standards of NIH for
136 care and use of animals. Animals were housed under a 12:12 h light-dark cycle, up to four
137 animals per cage with access to water and food *ad libitum*.

138

139 **Preparation and validation of α-Syn preformed fibrils**

140 The mouse α-Syn protein was purified using *Escherichia coli* BL21 codon plus RIPL cells
141 (RRID:CVCL_M639), which was then dialyzed using a buffer containing 10 mM Tris and 50 mM
142 NaCl (pH 7.5). A high-capacity endotoxin removal kit (PI88276) was used to remove the
143 endotoxins, the levels of which were assessed using an endotoxin quantification kit (A39552).
144 The protein concentration was estimated using absorbance at 280 nm with an extinction
145 coefficient of 7450 M^{-1} cm^{-1}. Purified mouse α-Syn monomer protein was used to generate
146 mouse α-Syn preformed fibrils (PFFs). Specifically, monomeric α-Syn protein was diluted to 5
147 mg/mL in the buffer, 150 mM KCl, 50 mM Tris-HCl and incubated at 37°C with shaking for 7 days,
148 as described previously [32]. After the incubation, sample was centrifuged for 10 min at 13,200
149 rpm. The protein pellet was re-suspended in half of the initial volume of the solution. To
150 estimate the fibril concentration, 5 µl of fibril solution was incubated with 5 µL of 8
151 M guanidinium chloride at room temperature for one hour. After incubation, the concentration

152 of PFF was measured using absorbance at 280 nm and diluted the PFF at 5 mg/mL and 22-25 µl
153 aliquots were stored at −80°C until use. Prior to the injection, PFF aliquot (22-25 µl at 5 mg/mL)
154 was thawed at room temperature and sonicated using Qsonica 700W cup horn sonicator at 30%
155 amplitude using 3 seconds on/2 seconds off cycle for 15 min at 15°C. The size of sonicated PFF
156 (30-70 nm segments) was estimated and confirmed using the dynamic light scattering (DynaPro
157 NanoStar from Wyatt technology). Detailed of generating and validating α-Syn PFFs can be
158 found here: dx.doi.org/10.17504/protocols.io.bhhrj356.
159

160 **Stereotaxic surgery**

161 Motorized stereotaxic frames were used for stereotaxic injections (Model# 51730M, Stoelting
162 Co.). Mice were anesthetized with 2% isoflurane and placed on a heating pad throughout the
163 surgery for maintenance of the body temperature. Eye ointment was administered to keep eyes
164 moisture and to protect them from strong light. To induce α-Syn pathology in mouse brain, we
165 bilaterally injected the sonicated PFFs (10 µg in a 2.0 µL volume) into the dorsal striatum
166 (anteroposterior (A-P), +0.2 mm from bregma; mediolateral (M-L), ± 2.0 mm from the midline;
167 dorsoventral (D-V), -2.9 mm from the brain surface) using a Nanoliter injector (NANOLITER2020,
168 World Precision Instrument) at a rate of 0.4 µL/min. To label the BLA principal neurons for
169 electrophysiological recordings, Retrobeads (LumaFluor Inc) were diluted (1:10 dilution) into
170 PFFs or PBS and then the mixed materials were co-injected into the dorsal striatum. Mice
171 injected with PBS or PBS plus beads at the same age were made as control groups. To
172 optogenetically evoke excitatory postsynaptic currents (EPSCs) of BLA projection neurons, we
173 injected 0.3 µL AAVs encoding ChR2(H134R)-eYFP (titer = 1 x 10^{12} GC/ml, Addgene# 26973,

174 RRID: Addgene_127090) into the layer 5 of medial prefrontal cortex (mPFC, A-P, +2.1 mm from
175 bregma; M-L, ± 0.3 mm from the midline; D-V, -2.3 mm from the brain surface) and the
176 centromedial thalamus (A-P, -1.5 mm from bregma; M-L, 0 mm from the middle; D-V, -3.3 mm
177 from the brain surface) at a rate of 0.1 µL/min. An intersectional approach was used for
178 selective activation of mPFC to BLA projection using chemogenetics: 1) retrograde AAV encoding
179 FlpO (0.3 µL, titer ≥ 7 x 10^{12} GC/ml, Addgene# 55637; RRID:Addgene_55637) were bilaterally
180 injected into BLA (A-P, -1.3 mm from bregma; M-L, ± 3.3 mm from the middle; D-V, -4.4 mm
181 from the brain surface), and 2) AAVs encoding FlpO-dependent excitatory designer receptors
182 exclusively activated by designer drugs (DREADDs) (titer = 2.5 x 10^{13} GC/ml, Addgene 154868;
183 RRID:Addgene_154868) were injected into infralimbic subregion of mPFC (IL-mPFC) (A-P, +2.1
184 mm from bregma; M-L, ± 0.3 mm from the midline; D-V, -2.6 mm from the brain surface).
185 Animals were returned to a cage placed on a warm pad after surgery and then housed in their
186 home cage until experiments. Details of this protocol can be found at:
187 dx.doi.org/10.17504/protocols.io.rm7vzye28lx1/v1
188
189 **Slice preparation for *ex vivo* physiological recording**
190 To prepare brain slices for physiological recording, mice were intraperitoneally injected with
191 avertin (300 mg/kg) for anesthesia, followed by transcardial perfusion using ice-cold, sucrose-
192 based artificial cerebrospinal fluid (aCSF), containing the follows (in mM): 230 sucrose, 26
193 $NaHCO_3$, 10 glucose, 10 $MgSO_4$, 2.5 KCl, 1.25 NaH_2PO_4, 0.5 $CaCl_2$, 1 sodium pyruvate, and 0.005
194 L-glutathione. Brain slices (300 µm thickness) with the BLA were collected using a vibratome
195 (VT1200S; Leica Microsystems, Buffalo Grove, IL) in the same sucrose-aCSF. Throughout the

196 preparation, brain slices were kept at about +4°C by a recirculating chiller (FL300; JULABO USA,
197 Inc, Allentown, PA). Then the slices were incubated at 35°C in regular aCSF bubbled with 95% O_2
198 and 5% CO_2 for 30 min (in mM, 126 NaCl, 26 $NaHCO_3$, 10 glucose, 2.5 KCl, 2 $CaCl_2$, 2 $MgSO_4$, 1.25
199 NaH_2PO_4, 1 sodium pyruvate, and 0.005 L-glutathione), and then kept at room temperature for
200 at least another 30 min prior to recording. Details of this procedure can be found here:
201 https://www.protocols.io/view/protocol-for-obtaining-rodent-brain-slices-for-ele-
202 ewov1y7mpvr2/v2
203

204 **Slice electrophysiology recording and optogenetics**

205 Brain slices were transferred to recording chamber with modified aCSF (in mM, 126 NaCl, 26
206 NaHCO3,10 glucose, 3 KCl, 1.6 $CaCl_2$,1.5 $MgSO_4$, and 1.25 NaH_2PO_4), which was equilibrated
207 with 95% O_2 and 5% CO_2 at 32–34°C via a feedback-controlled in-line heater (TC-324C, Warner
208 Instruments). A gradient contrast SliceScope 1000 (Scientifica, UK) with an IR-2000 CCD camera
209 (DAGE-MTI, USA) using infrared illumination was used to visualize neurons in slices. A motorized
210 micromanipulator was used to control the position of the glass pipette for recording. The BLA
211 principal cells were identified based on the presence of somatic Retrobeads signals under a 60x
212 water immersion object lens (Olympus, Japan).

213 Electrophysiology data were collected using an Axon 700B amplifier and digitized with a
214 1550B digitizer (Molecular Devices, San Jose, USA). Signals were low pass filtered at 2 kHz and
215 sampled at 50 kHz under the control of pClamp 11 (RRID: SCR_011323, Molecular Devices, San
216 Jose, USA). Borosilicate glass pipettes with resistance at 4-6 MΩ (O.D. = 1.5 mm, I.D. = 0.86, item
217 # BF150-86-10, Sutter Instruments, Novato, CA) were made by a micropipette puller (P1000,

218 Sutter Instruments, Novato, CA). For voltage-clamp recordings of synaptic transmission, a Cs^+-
219 based intracellular solution containing the following (in mM): 120 CH_3O_3SCs, 2.8 NaCl, 10 HEPES,
220 0.4 Na_4-EGTA, 5 QX314-HBr, 5 phosphocreatine, 0.1 spermine, 4 ATP-Mg, and 0.4 GTP-Na was
221 used; the pH was adjusted to pH 7.3 with CsOH. A K-gluconate-based internal solution (in mM,
222 140 K-gluconate, 3.8 NaCl, 1 MgCl2, 10 HEPES, 0.1 Na_4-EGTA, 2 ATP-Mg, and 0.1 GTP-Na, 0.2%
223 Biocytin, pH 7.3, 290 mOsm) was used to label the BLA projections neurons for morphology
224 studies using Cy-streptavidin. For optogenetic stimulation, light pulses with 1 ms duration were
225 delivered through a 60x objective lens (Olympus, Japan) using a 470 nm LED light illumination
226 (CoolLED, UK). TTX (1 µM) and 4-AP (100 µM) were perfused to isolate monosynaptic mPFC-BLA
227 neurotransmission. To measure the synaptic strength, peak amplitude of AMPARs-mediated
228 EPSCs at -80 mV were calculated. Paired-pulse ratio at 10 Hz was quantified as the ratio of
229 amplitude between the second EPSCs over the first EPSCs (i.e., EPSC2/EPSC1). To measure
230 AMPA/NMA ratio, NMDA-mediated current at +40 mV was measured at 50 ms after optogenetic
231 stimulation when AMPAR mediated-EPSCs decayed to the baseline. Series resistance (R_s) was
232 continuously monitored during recordings and only cells showed stable R_s < 20 MΩ with less
233 than 15% changes were proceeded for further analysis. Details of this procedure can be found
234 here: https://www.protocols.io/view/brain-slice-preparation-for-electrophysiology-reco-
235 36wgqj2eovk5/v1
236

237 **Perfusion and immunohistochemistry staining**

238 Mice were intraperitoneally injected with avertin for anesthesia followed by transcardial
239 perfusion using 1x PBS and 4% paraformaldehyde (PFA, pH = 7.4). After perfusion, the brains

240 were extracted and kept in 4% PFA overnight for post-fixation, and then were re-sectioned at a
241 70 µm thickness using a vibratome (VT1000s, Leica Biosystems, Buffalo Grove, IL).
242 https://www.protocols.io/view/standard-operating-procedure-mouse-transcardiac-pe-
243 3byl4b8r8vo5/v1
244
245 Brain sections were rinsed with 1x PBS for 3 times before performing
246 immunohistochemistry, followed by incubation with 1x PBS containing 0.5% Triton X-100 (PBS-T)
247 plus 2% normal donkey serum (Millipore Sigma) at room temperature for 60 min. They were
248 then incubated in the PBS-T with primary antibodies overnight at room temperature or 48 hours
249 at 4°C. The primary antibodies utilized in this study were: rabbit anti-pS129 α-Syn (1:10,000,
250 Bioscience Cat# 1536-1, RRID: AB_562180), mouse anti-NeuN (1:500, Millipore Cat# MAB377,
251 RRID: AB_2298772), mouse anti-vGluT1 (1:1,000, Synaptic Systems Cat# 135 011,
252 RRID:AB_2617087), guinea pig anti-vGluT2 (1:1,000, Synaptic System Cat# 135404, RRID:
253 AB_887884). The sections were then thoroughly rinsed with 1x PBS for 3 times before
254 incubating with the secondary antibodies (1: 500, AlexaFluor 594 donkey anti-rabbit IgG, Cat#
255 711-585-152, Jackson ImmunoResearch Labs, RRID: AB_2340621; AlexFluor 594 donkey anti-
256 mouse IgG, Cat# 715-586-150, Jackson ImmunoResearch Labs, RRID: AB_2340857; AlexaFluor
257 488 donkey anti-guinea pig IgG, Cat# 706-545-148, Jackson ImmunoResearch Labs, RRID:
258 AB_2340472) at room temperature for 2 hours. To reveal morphology of biocytin-labeled
259 neurons, brain slices were incubated with Cy5-conjugated streptavidin (SA1011, Thermo Fisher
260 Scientific) at a concentration of 1: 500 at room temperature for 2 h. Brain slices were then
261 rinsed using 1x PBS for 3 times before mounting on glass slides with the Vectorshield antifade

262 mounting medium (H-1000, Vector Laboratories). Slides were left at room temperature
263 overnight before sealing with nail oil and imaging. Details of immunofluorescent staining can be
264 found here: https://www.protocols.io/view/immunofluorescent-staining-3byl4bq9ovo5/v1
265

266 **Confocal imaging and analysis**

267 Confocal images were taken using a Nikon A1R microscope. Images of α-Syn pathology in BLA
268 were collected by a 20x objective lens and then analyzed using imageJ (RRID: SCR_003070, NIH,
269 https://imagej.net). To quantify the cortical and thalamic axon terminals in the BLA, vGluT1 and
270 vGluT2 immunoreactivity were imaged using a Nikon A1R confocal microscope under an oil
271 immersion 100x objective lens (NA=1.45; x/y, 1024 x 1024 pixels; z-step = 150 nm). All confocal
272 images were acquired using the identical microscope and camera settings. VGluT1 and vGluT2
273 density were stereologically quantified using optical dissector methods (dissector height = 3 µm
274 with a guard zone of 0.15 µm; counting frame = 10 x 10 µm) [33]. Images of NeuN staining were
275 taken from the BLA by a 60x objective (NA=1.40; x/y, 1024 x 1024 pixels; z-step = 1 µm) and
276 subjected to quantification using Imaris software (RRID: SCR_007370, version 10.0, Oxford, UK,
277 https://imaris.oxinst.com). ChR2-eYFP expression in mPFC was imaged using a Nikon Ni-U
278 fluorescence microscope under 2x objective lens. For morphology analysis, biocytin-filled
279 neurons were imaged using the confocal microscope under 20x objective lens (NA=0.75; x/y,
280 1024 x 1024 pixels; z-step = 1 µm). Morphology of biocytin-labelled neurons of BLA was
281 reconstructed followed by Sholl analysis using the Imaris software (RRID: SCR_007370, version
282 10.0, Oxford, UK, https://imaris.oxinst.com). Spines of the biocytin-filled neurons were imaged
283 by the confocal microscope under 100x objective lens (NA=1.45; x/y, 1024 x 1024 pixels; z-step =

284 500 nm). To quantify the spine density of BLA neurons, dendritic segments of 20 µm in length
285 were reconstructed and number of spines were counted. Images from controls and PFFs
286 injected mice were collected under identical settings in the confocal microscope and analyzed
287 by a researcher blinded to treatments. Details of digital imaging analysis can be found here:
288 https://www.protocols.io/view/confocal-imaging-and-digital-image-analysis-3byl4jmxzlo5/v1.
289

290 **Animal behaviors**

291 To assess motor function, animals were subject to locomotion and rotarods tests. For open field
292 locomotion test, the animal was placed in the empty open field (40 x 40 x 30 cm, W x L x H) and
293 allowed to explore for 10 min. Animal's locomotor activity was continuously recorded and
294 analyzed using ANYmaze software (RRID:SCR_014289, Stoelting Co., Wood Dale, IL;
295 http://www.sandiegoinstruments.com/any-maze-video-tracking/). For rotarod test, the animal
296 was placed on an accelerating rod (speed of 4-40 rpm in 5 min, San Diego Instruments, CA) and
297 the latency of fall was monitored and recorded. Detailed protocol of motor activity assays can
298 be found here: https://www.protocols.io/view/open-field-locomotion-test-e6nvwjxmdlmk/v1.
299 To assess animals' social interaction behavior, mice were placed to three-chamber apparatus
300 (MazeEngineers, Skokie, IL) with left, middle, and right chambers (20 x 13.5 cm^2). A round wire
301 cage (10 cm in diameter, 20 cm in height) was placed in the left and right chambers for novel
302 stimulus mouse. The stimulus mice were habituated to the wire cages for 20 min before the
303 testing day. The testing mice were habituated to the behavior room for at least 30 min before
304 the experiment. Three sessions were conducted during the testing day, including the
305 habituation, the session 1, and the session 2. The testing mice were habituated to the middle

306 chamber for 5 min before opening the doors to allow the mice freely explore the three
307 chambers for 10 min. During the first session, the testing mice were allowed to explore the
308 three chambers for a total of 10 min with one empty cage and the presence of a stimulus
309 mouse in the other wire cage. In the second session, the same testing mouse was allowed to
310 explore the three chambers for another 10 min with the presence of the familiar mouse in one
311 cage and a second never-met stimulus mouse in another wire cage. Mice movements were
312 tracking and the time spent in each chamber was quantified by AnyMaze software
313 (RRID:SCR_014289, Stoelting Co.). Between each testing, the chamber was thoroughly cleaned
314 with 70% ethanol to eliminate the odor of mice.
315
316 **Data analysis and statistics**
317 Electrophysiology data were analyzed using Clampfit 11.1 (RRID: SCR_011323, Molecular
318 Devices, San Jose, USA). The amplitude of monosynaptic glutamatergic EPSCs were quantified
319 from an average of three sweeps. Confocal images were analyzed using Image J (RRID:
320 SCR_003070, NIH, https://imagej.net) and Imaris (RRID: SCR_007370, Oxford, UK,
321 http://www.bitplane. com/imaris). Statistics were performed in Prism 10 (RRID: SCR_002798,
322 GraphPad Software, http://www.graphpad.com). Non-parametric, distribution-independent
323 Mann-Whiney U (MWU) test was used for statistical comparison of data from two groups. The
324 amplitude of Cortico-BLA EPSCs across a range of stimulation and Sholl analysis were analyzed
325 using two-way analysis of variance (ANOVA) with *post hoc* Sidak's analysis multiple comparison's
326 test. All tests were two-tailed, and p-value < 0.05 was considered as statistical significance.

327 **Results**

328 **Time-course of α-Syn pathology development in the BLA**

329 We injected α-Syn PFFs into the dorsal striatum of wildtype C57BL6 mice to induce the
330 accumulation of α-Syn pathology in the brain, including the cerebral cortical regions and the
331 amygdala [3, 25, 31]. In the PFFs-based models, fibrillar α-Syn species are reported to be
332 internalized at the axon terminals, which then recruit endogenous α-Syn to form insoluble
333 inclusions and eventually result in neurodegeneration [3, 11, 16].

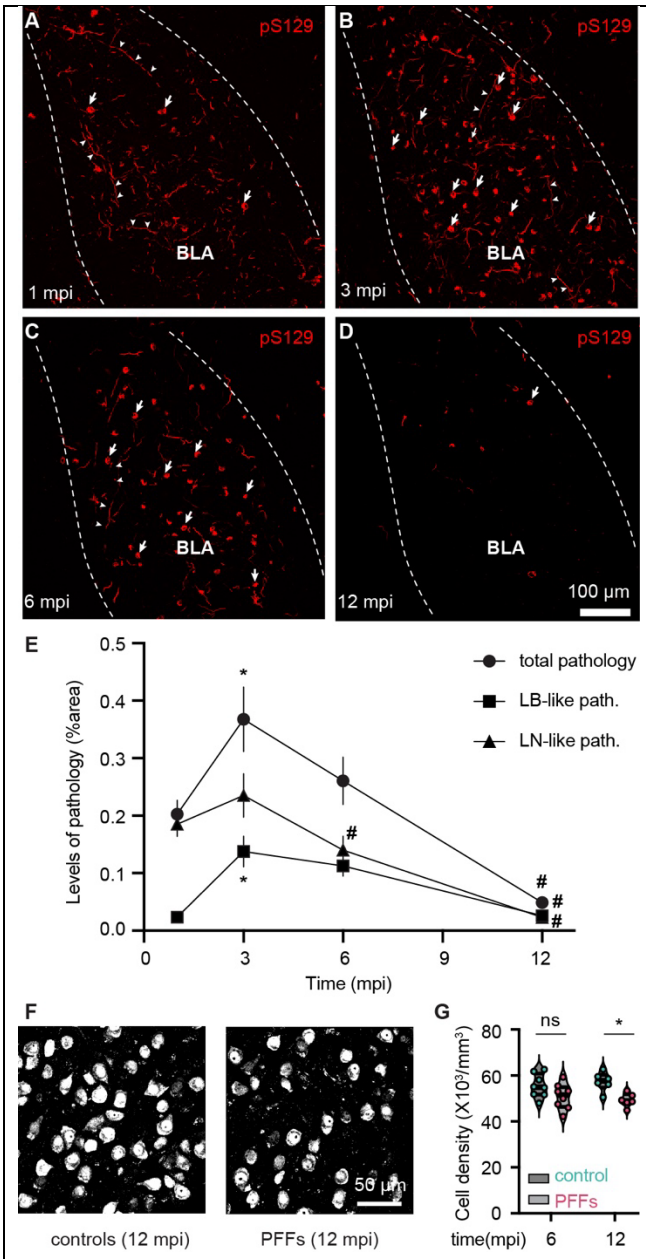

Figure 1. Time-course of αSyn pathology development in the BLA. A-D) Representative confocal images showing the development and accumulation of pS129⁺ pathology in the BLA at 1, 3, 6 and 12 months-post-injection (mpi). Arrows and arrowheads highlighted a few pS129⁺ somatic aggregates and neurites, respectively, in the BLA. **E)** Time course of the development of total α-syn pathology (filled circles), LB-like pS129⁺ pathology (square), and LN-like pS129⁺ pathology (triangle) in the BLA. Total α-Syn pathology, 1 mpi = 0.20±0.02, n = 38 slices/8 mice; 3 mpi = 0.37±0.06, n = 28 slices/10 mice; p = 0.004. LB-like pS129⁺ pathology, 1 mpi =0.02±0.005, n = 38 slices/8 mice; 3 mpi =0.14±0.03, n = 28 slices/10 mice, p < 0.0001. LN-like pS129⁺ pathology, 1 mpi =0.19±0.02, n = 38 slices/8 mice, 3 mpi = 0.24±0.04, n = 28 slices/10 mice, p = 0.3. Total α-Syn pathology at 6 mpi = 0.26±0.04, n = 38 slices/10 mice, p = 0.09 versus total pathology at 3 mpi. LB-like pS129⁺ pathology at 6 mpi = 0.11±0.02, n = 38 slices/10 mice, p = 0.5 versus LB-like pS129⁺ pathology at 3 mpi. LN-like pS129⁺ pathology at 6 mpi = 0.14±0.02, n = 38 slices/10 mice, p = 0.01 versus LN-like pS129⁺ pathology at 3 mpi. Total α-Syn pathology at 12 mpi = 0.05±0.007, n = 35 slices/6 mice, p < 0.0001 versus total pathology at 3 mpi. LB-like pS129⁺ pathology at 12 mpi = 0.026±0.005, n = 35 slices/6 mice, p < 0.0001 versus LB-like pS129⁺ pathology at 3 mpi. LN-like pS129⁺ pathology at 12 mpi = 0.02±0.0035, n = 35 slices/6 mice, p < 0.0001 versus LN-like pS129⁺ pathology at 3 mpi. *p< 0.05 relative to the counterparts at 1 mpi, #p < 0.05 relative to the counterparts at 3 mpi; one-way ANOVA. **F**) Representative images showing NeuN immunoreactivity in the BLA of controls and PFFs-injected mice at 12 mpi. **G**) Summarized results showing a reduced BLA cell density in the PFFs-injected mice relative to controls at 12 mpi, but not at the 6 mpi. Cell densities at 6 mpi, control = 54.9 [51.7, 60.8] $x10^3/mm^3$, PFFs = 51.5 [46.4, 54.9] $x10^3/mm^3$, n = 8 mice/group, p = 0.16; Cell densities at 12 mpi, control = 57.7 [54.7, 60.3] $x10^3/mm^3$, PFFs = 48.9 [47.4, 51.8] $x10^3/mm^3$, n = 6 mice/group, p = 0.0087, Mann-Whitney U (MWU) test.

334

335 As expected, we detected robust phospho-Ser129 (pS129$^+$) α-Syn immunoreactivity in
336 the BLA of PFFs-injected mice (**Figure 1A-D**), but not in the BLA of PBS- or monomer-injected
337 controls ("controls" hereinafter). α-Syn pathology in the BLA included both pS129$^+$ Lewy neurite
338 (LN)-like and large Lewy body (LB)-like aggregates (**Figure 1A-D**), which are likely the α-Syn
339 pathology within cortical afferents of the BLA and the cytoplasmic aggregates within
340 glutamatergic principal neurons of the BLA, respectively [31, 34]. Next, we characterized the
341 dynamic changes of α-Syn pathology abundance in the BLA at 1, 3, 6, and 12 months-post-
342 injection (mpi). We measured the proportion of the BLA region covered by LN- and LB-like
343 pS129$^+$ aggregation, as well as their combination as the total α-Syn pathology (i.e., pS129$^+$
344 LN/LB-like aggregates, **Figure 1E**) [25, 26]. Specifically, moderate level of pS129$^+$ α-Syn
345 pathology was detected in the BLA as early as at 1 mpi, which was dominated by the LN-like
346 pS129$^+$ aggregates (**Figure 1A, E**). The level of total pS129$^+$ α-Syn pathology continually grew
347 beyond 1 mpi, peaking at 3 mpi (**Figure 1B, E**). After 3 mpi, the amount of total α-Syn pathology
348 in the BLA remained at a relatively high at the 6 mpi timepoint but decreased significantly at 12
349 mpi (**Figure 1C, D, E**). Particularly, at 12 mpi only few LB-like pS129$^+$ aggregates could be seen in
350 the BLA (**Figure 1D, E**).
351
352 Post-mortem studies of patients with advanced PD reported that the amygdala exhibits
353 significant Lewy body pathology and reduced cell density [24]. Consistently, using unbiased
354 stereological counting of pan-neuronal marker NeuN, we detected a significant reduction of the
355 NeuN density in the BLA at 12 mpi relative to controls, but not at 6 mpi (**Figure 1F, G**, see also
356 [31]). These data are consistent with the loss of cortical glutamatergic neurons and midbrain

357 dopaminergic neurons driven by the formation and maturation of LB-like pS129$^+$ aggregates [3,
358 11, 35]. Together the above results suggest that robust reduction in the LB-like pS129$^+$
359 aggregates at 12 mpi was, at least partially, due to neuronal loss in the BLA.
360
361 **Loss of cortical afferents contributes to the decreased pS129$^+$ neurites in the BLA**
362 Glutamatergic inputs from the cerebral cortex and the thalamus are the major excitatory drive
363 of the BLA neuronal activity and they form synapses with the spines and dendrites of BLA
364 principal neurons. Interaction of cortical and thalamic inputs is critical to proper manifestation
365 of emotion and behavior. Our recent study suggest that cortical and thalamic axons show
366 distinct functional vulnerability to α-Syn aggregation at 1 month post PFFs injections when there
367 was no overt loss of glutamatergic axonal terminals. It remains to be determined whether and
368 when α-Syn aggregates induce loss of cortical and/or thalamic inputs in the BLA. Thus, we
369 rigorously examined cortical and thalamic inputs to the BLA at additional time points in both
370 controls and PFFs-injected mice.
371 Cortical and thalamic axon terminals can be distinguished by their preferential
372 expression of vesicular glutamate transporter (vGluT) 1 and 2, respectively. Using optical
373 dissector methods, we stereologically quantified the density of vGluT1$^+$ puncta in the BLA,
374 starting from 3 mpi when the level of LN-like pS129$^+$ α-Syn aggregation reached a peak (**Figure**
375 **1E**). Although pS129$^+$ α-Syn was tremendous in the BLA at 3 mpi, there was no change in the
376 density of vGluT1$^+$ puncta (**Figure 2A**). However, a significant reduction in the density of vGluT1$^+$
377 puncta in the BLA was detected at 6 mpi (**Figure 2B**), indicating a gradual loss of cortico-BLA

378 axonal projections at later time points, though a downregulation of vGluT1 protein itself cannot

379 be excluded.

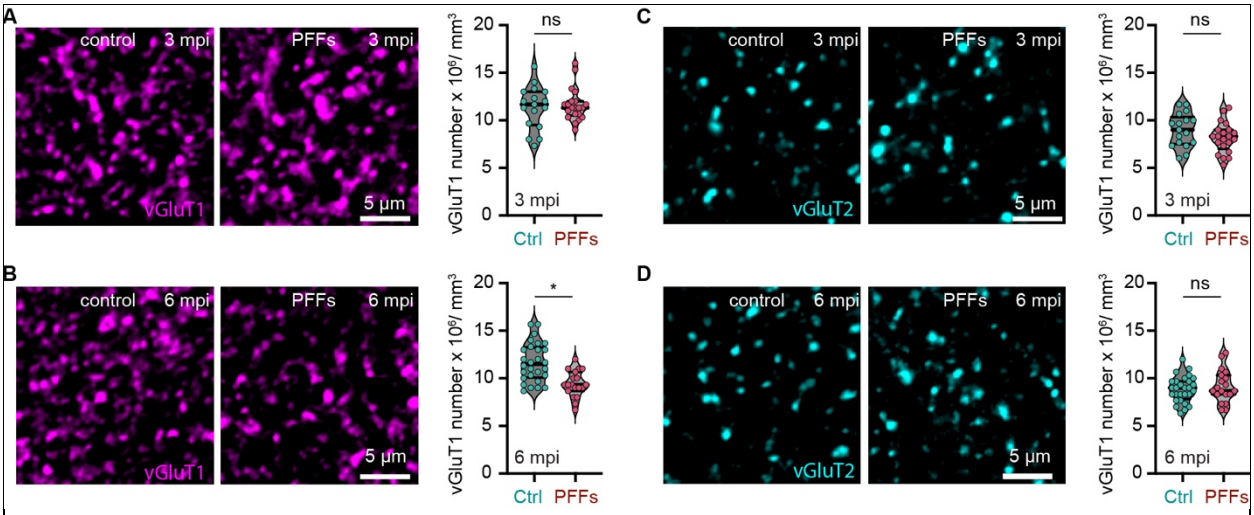

Figure 2. Loss of cortical afferents contributes to the decreased pS129⁺ neurites in the BLA. A-B) *Left*, representative confocal images showing vGluT1 immunoreactive puncta in the BLA of controls and PFFs-injected mice at 3 and 6 mpi. *Right*) Summarized result showed changes in vGluT1 densities in the BLA at 3 and 6 mpi. *A,* vGluT1 densities at 3 mpi, controls = 11.7 [9.5, 13], PFFs = 11.3 [10.5, 12.0], p = 0.86. *B,* vGluT1 densities at 6 mpi, controls = 11.5 [10.1, 13.3], PFFs = 9.3 [8.7, 10.7], p = 0.0001. **C-D**) *Left*, representative confocal images showing vGluT2 immunoreactive puncta in the BLA of controls and PFFs-injected mice at 3 and 6 mpi. *Right*) Summarized result showed no change in vGluT2 densities in the BLA at 3 and 6 mpi. *D,* vGluT2 densities at 3 mpi, controls = 9.0 [7.5, 10.3], PFFs = 8.3 [7.0, 9.0], p = 0.1387. *E,* vGluT2 densities at 6 mpi, controls = 9.0 [7.8, 9.7], PFFs = 8.7 [8.3, 10.3], p = 0.4883. N = 21 slices/4 mice for each group at 3 mpi, 19 slices/4 mice for each group at 6 mpi. MWU test.

380

381 When it came to thalamic inputs to the BLA, we found no change in the density of

382 vGluT2⁺ puncta in the BLA of PFFs injected mice relative to respective controls at 3 and 6 mpi

383 (**Figure 2C, D**). These data indicate that thalamic-BLA axonal projections were not altered by the

384 α-Syn pathology in the brain. Taken together, we concluded that the reduction of LN-like pS129⁺

385 aggregates in the BLA between 3 mpi and 6 mpi was mainly due to a loss of cortical axonal

386 inputs, but not the thalamic afferents.

387 Given the cortical inputs mainly target dendritic spines of BLA principal neurons, loss of

388 cortical axonal terminals is expected to be accompanied by a reduction of postsynaptic spines.

389 Thus, we further quantified the density of dendritic spines of the biocytin labeled BLA principal

390 neurons that were retrogradely labeled by intrastriatal injection of Retrobeads and PFFs mixture

391 (**Figure 3A, B**). We found that BLA principal neurons exhibited a reduced density of dendritic

392 spines at 3 and 6 mpi (**Figure 3C-F**).

393 Taken together, α-Syn aggregation triggers loss of presynaptic cortical axon terminals and

394 postsynaptic dendritic spines of BLA principal neurons, which is likely to result in a loss of

395 cortico-BLA synapses as α-Syn pathology accumulates in the brain, e.g. at 6 mpi.

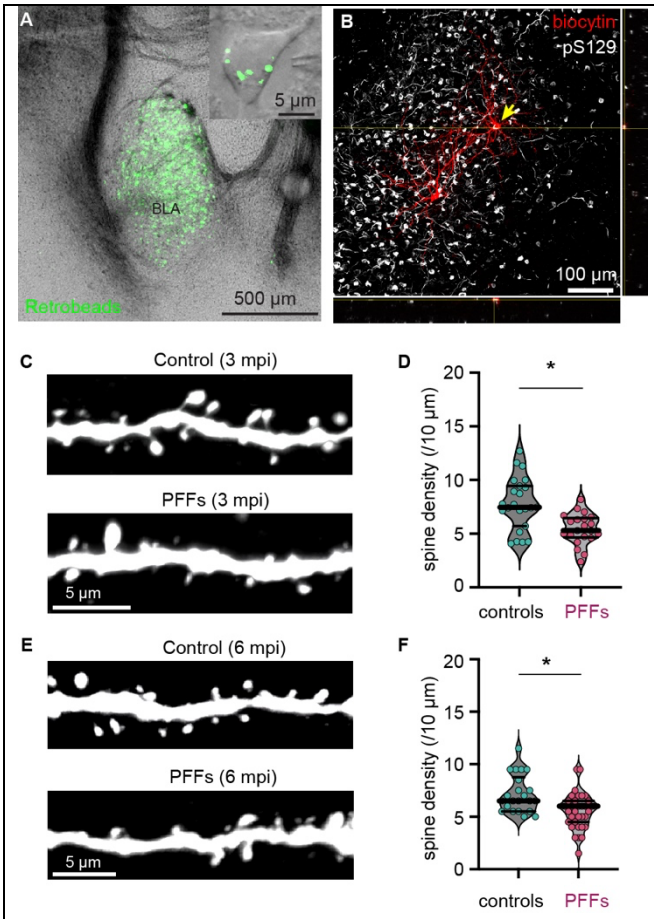

Figure 3. Loss of dendritic spines of the BLA principal neurons as α-Syn pathology develops. A) Representative images showing green Retrobeads-labeled BLA neurons at low and high (inset) magnification. Cells with green beads labeling were targeted for biocytin filling and morphology analysis. **B**) Representative image showing a Cy5-labeled BLA principal neurons against pS129^{+} α-Syn immunoreactivity. This cell showed clear somatic aggregation of pS129^{+} α-Syn. **C**) Confocal images showing representative dendritic spines of BLA neurons from controls and PFFs-injected mice at 3 mpi. **D**) Summarized results showing reduced dendritic spine densities of BLA neurons from PFFs-injected mice relative to control at 3 mpi. **E-F**) Similar to (C-D) but at 6 mpi. Spine densities at 3 mpi, controls = 7.45 [5.7, 9.44]/10 µm; PFFs = 5.3 [4.66, 6.46]/10 µm, n= 21 segments/4 mice, p = 0.0008, MWU; Spine densities at 6 mpi, controls = 6.5 [5.5, 8.75]/10 µm, PFFs = 6.0 [4.5, 6.5]/10 µm, n = 36 segments/4 mice, p = 0.002, MWU.

396

397 **α-Syn pathology disrupts cortico-BLA functional connectivity prior to loss of synapses**

398 After establishing a time course of neuronal and synaptic losses in the BLA, we next assessed
399 the functional connectivity between the cerebral cortex and the BLA. The medial prefrontal
400 cortex (mFPC) and the BLA form interconnected microcircuits that play a critical role in
401 regulating social behavior [36-38]. Both the mPFC and the BLA accumulate robust α-Syn
402 pathology following intrastriatal PFFs injection[3, 31], the functional connectivity of mPFC-BLA
403 pathway is expected to be impaired. Thus, we assessed how α-Syn pathology affects mFPC-BLA
404 connection at 3 and 6 mpi when the abundance of α-Syn pathology remained high but has
405 caused no or subtle degeneration of BLA neurons and presynaptic cortical axonal terminals
406 (**Figures 1 and 2**). We virally expressed AAV9-hSyn-ChR2(H134R)-eYFP in the layer 5 projection
407 neurons of the mPFC, allowing a selective activation of mPFC-BLA inputs (**Figure 4A**). We
408 optogenetically stimulated ChR2(H134R)-expressing axon terminals in the BLA (**Figure 4A**) and
409 recorded the evoked excitatory postsynaptic currents (EPSCs) in the retrogradely labeled BLA
410 principal neurons under the voltage-clamp mode from controls and PFFs-injected mice (**Figure**
411 **4B, C**). The amplitude of optogenetically-evoked, monosynaptic EPSCs were quantified to assess
412 the connection strength of mPFC-BLA synapses. A significant reduction of the amplitude of
413 mPFC-BLA EPSCs was detected in PFFs-injected mice relative to control at both 3 and 6 mpi
414 (**Figure 4B, C**), indicating a reduced connection strength of the mPFC-BLA synapses.
415 The reduced connection strength of mPFC-BLA synapses was accompanied by a
416 decreased ratio of amplitude of EPSCs mediated by AMPA receptors and NMDA receptors (i.e.,
417 AMPA/NMDAR ratio) in PFFs-injected mice relative to controls at both 3 and 6 mpi (**Figure 4D-**
418 **F**). Moreover, the ratio of EPSC2/EPSC1 at the mPFC-BLA synapses evoked by paired optogenetic
419 stimulation was also decreased in PFFs-injected mice relative to controls at both 3 and 6 mpi

420 (**Figure 4G-I**), indicating an enhanced initial release probability of neurotransmitter at mPFC-BLA

421 input. Together with the time course of synaptic marker changes (**Figures 2 and 3**), these data

422 demonstrated that α-Syn pathology decreases the connection strength of cortico-BLA pathway

423 at 3 mpi prior to a robust loss of cortico-BLA synapses at 6 mpi.

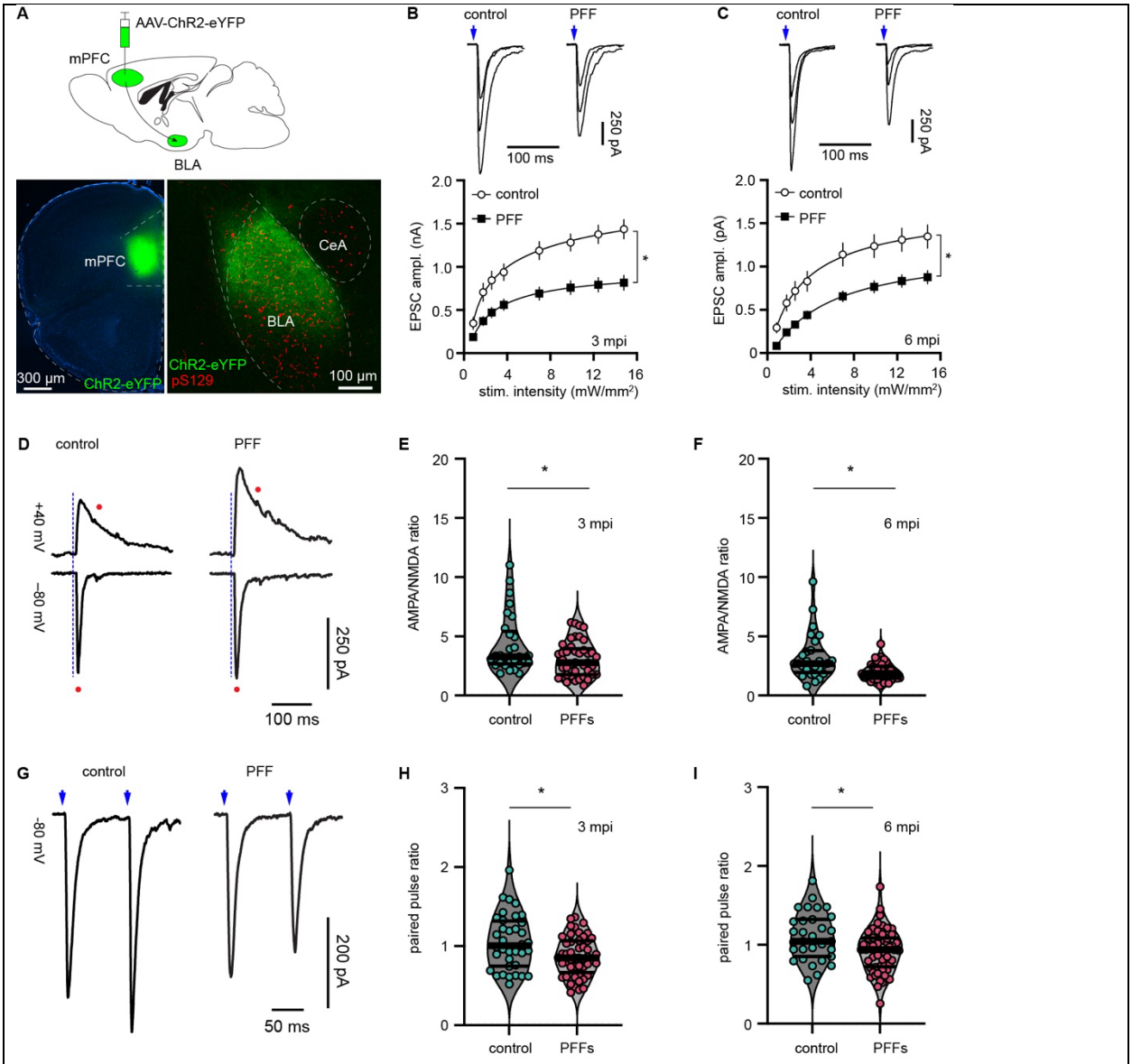

Figure 4. α-Syn pathology disrupts functional connectivity of the mPFC-BLA synapses. A) *Top*, diagram showing overall experimental design. *Bottom*, Representative AAV-ChR2-eYFP injection site in the mPFC (left) and the eYFP-labeled axonal terminal field in the BLA (right). **B-C**) Decreased amplitude of optogenetically evoked mPFC-BLA EPSCs in PFFs-injected mice relative to controls at both 3 (B) and 6 (C) mpi. *Top*) Representative traces of EPSCs evoked by optical stimulation intensities of 1.8, 3.6, and 12 mW/mm^2. Blue arrows indicate when the optogenetic stimulation was delivered. *Bottom*) Summarized graphs showing reduced amplitude of mPFC-BLA ESPCs across a

range of stimulation intensities in PFFs-injected mice relative to controls at both 3 and 6 mpi. N = 44 cells/7 mice at 3 mpi and 57 cells/7 mice at 6 mpi. Two-way ANOVA followed by Sidak multiple comparisons test. **D**) Representative traces of mPFC-BLA EPSCs recorded at -80 mV and +40 mV from both controls and PFFs-injected mice. Red dots indicate where the AMPA receptor- and NMDA receptor-mediated EPSCs were measured at -80 mV and +40 mV, respectively. Blue dashed lines indicate when optogenetic stimulation was delivered. **E-F**) Summarized result showing reduced AMPA/NMDA ratios at mPFC-BLA synapses in PFFs-injected mice relative to controls at 3 mpi (E, control = 3.3 [2.7, 5.4], n = 29 cells/4 mice, PFFs = 2.8 [1.8, 4.0], n = 41 cells/7 mice, p = 0.05) and 6 mpi (F, control = 2.7 [1.9, 3.8], n = 28 cells/4 mice, PFFs = 1.9 [1.5, 2.5], n = 46 cells/6 mice, p = 0.0006) . **G**) Representative traces of mPFC-BLA EPSCs evoked by paired optogenetic stimulation pulses at -80 mV in both controls and PFFs-injected mice. Blue arrows indicate when the optogenetic stimulation was delivered. **H-I**) Summarized results showing reduced ratios of EPSC2/EPSC1 at the mPFC-BLA synapses in PFFs-injected mice relative to controls at both 3 mpi (H, control = 1 [0.75, 1.32], n = 36 cells/5 mice; PFFs = 0.85 [0.67, 1.1], n = 48 cells/7 mice, p = 0.016, MWU) and 6 mpi (I, control = 1.04 [0.85, 1.32], n = 31 cells/4 mice, PFFs = 0.94 [0.72, 1.09], n= 57 cells/7 mice, p = 0.008, MWU test).

Social interaction behavior is impaired by α-Syn pathology and rescued by chemogenetic activation of mPFC-BLA pathway

Given the functional disconnection between the mPFC and the BLA at 3 mpi (**Figure 5**), we next attempted to determine whether the impaired mPFC-BLA projection affects amygdala-dependent behavior. We performed behavioral tests using both controls and PFFs-injected mice at 3 mpi when the α-Syn pathology remained at peak levels but has not yet resulted in significant neuronal or synaptic losses in the BLA (**Figures 2 and 3**), making functional rescue still possible. We chose the 3-chamber sociability test, as the performance in this test is dependent on an intact amygdala microcircuit as well the interaction between the BLA and the mPFC [36, 39, 40]. Each test began with 10 min habituation to the behavior apparatus with two empty cages. During the habituation, both controls and PFF-injected mice spent comparable amount of time in the left and right chambers of the empty cage. This result indicates that neither controls nor PFFs-injected mice exhibited baseline preference of either chamber. Next, a stimulus mouse was placed into one empty cage (S1, **Figure 5A**), and the test mouse was then allowed to explore both chambers (session I in **Figure 5A**). Both controls and PFF-injected mice spent

440 significantly more time with the never-before-met stimulus mouse S1 than that with the non-
441 social empty cage (**Figure 5A, B, D**). This result suggests that PFFs-injected mice exhibit normal
442 sociability relative to controls. Next, we studied social novelty preference of PFFs-injected mice.
443 To do this, we added a second novel stimulus mouse 2 (S2) into the empty cage in the presence
444 of the familiar stimulus S1 to evaluate the test mouse's interest in the familiar social stimulus
445 *versus* the novel one when both were present (see the session 2 in **Figure 5A, C**). While controls
446 spent much more time with the novel stimulus (S2) relative to the familiar one (S1), PFFs-
447 injected mice spent similar amount of time with either the familiar stimulus (S1) or the novel
448 stimulus (S2) (**Figure 5C, E**).
449 It is important to note that relative to controls, PFFs-injected mice at 3 mpi showed
450 comparable general motor activity in locomotion test and rotarod test and similar levels of
451 anxiety elevated plus maze as measured by the time spent in open arms (**Supplementary Figure**
452 **1**). These data were consistent with previous report [3, 25, 31] and suggested that PFFs-injected
453 mice do not develop parkinsonian motor deficits or enhanced anxiety, which is important as
454 such behaviors could confound the social interaction behavioral test. Taken together, these
455 results suggested that PFFs-injected mice exhibited impaired social novelty preference and were
456 not able to distinguish between familiar- and novel-stimuli.
457

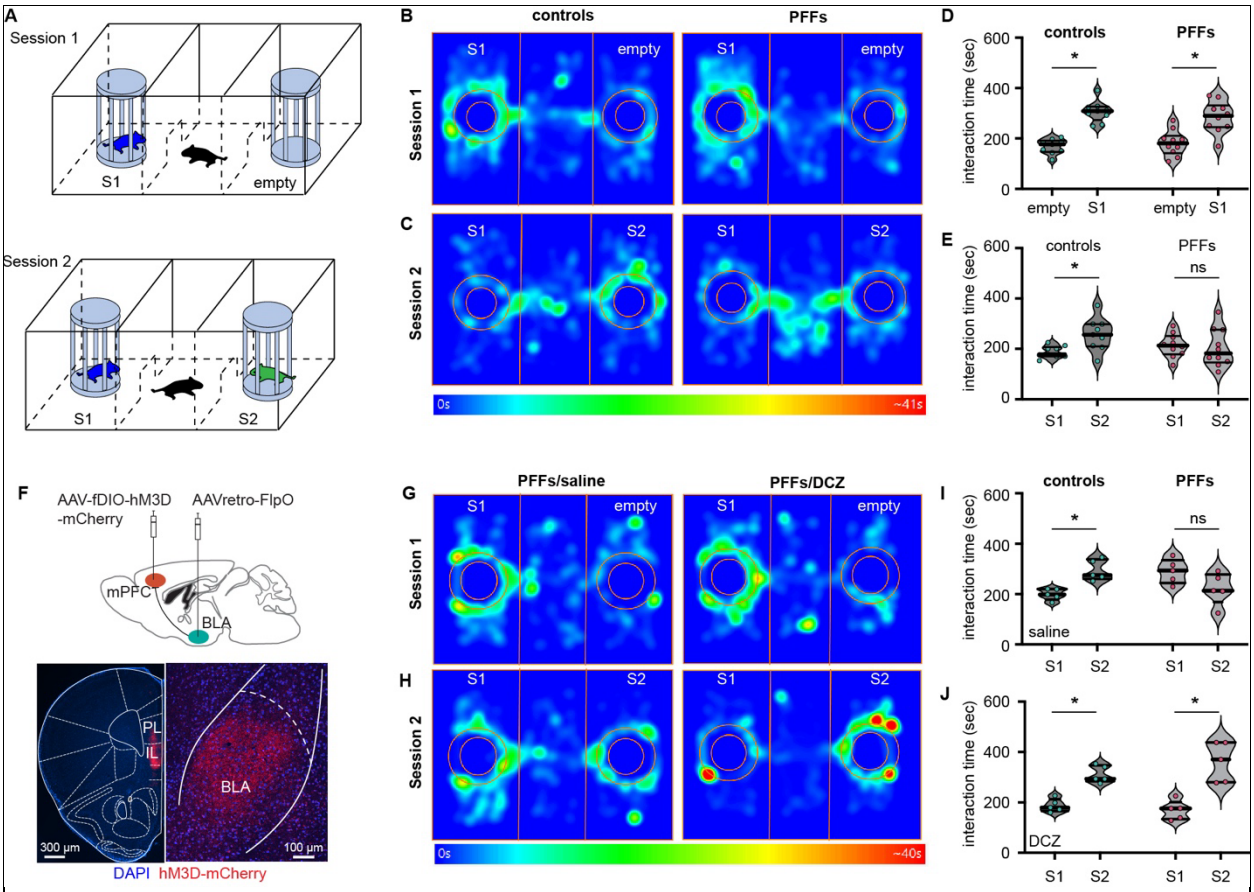

Figure 5. Social interaction behavior was impaired by α-Syn pathology and rescued by chemogenetic activation of mPFC-BLA pathway. A) Diagram showing overall behavioral experimental design. **B**) Representative heatmap plots showing social interaction behavior of controls and PFFs-injected mice in the Session 1 when S1 was paired with an empty cage for sociability. **C**) Representative heatmap plots showing social interaction behavior of controls and PFFs-injected mice in the Session 2 when familiar S1 was paired with a novel stimulus S2 for social novelty preference. **D-E**) Summarized graphs showing a normal sociability (D, controls empty = 177 [147, 191] sec, control S1 = 309 [273, 326] sec, n = 9 mice, $p < 0.0001$; PFFs empty = 181 [142, 211] sec, PFFs S1 = 290 [245, 331] sec, n = 10 mice, p = 0.001, MWU) but impaired social novelty preference behavior of PFFs-injected mice relative to controls (E, control S1 = 179 [170, 207] sec, control S2 = 256 [210, 298] sec, n= 9 mice, p = 0.01, MWU; PFFs S1 = 213 [179, 251] sec, PFFs S2 = 182 [146, 276] sec, n = 10 mice, p = 0.49, MWU). **F**) Representative image showing AAV-fDIO-hM3D(Gq)-mCherry infection site in the mPFC and the mCherry-labeled mFPC-BLA axon terminal field. **G**) Representative heatmap plots showing sociability of PFFs-injected mice receiving either saline or DCZ (DREADDs agonist) administration. **H**) Representative heatmap plots showing social novelty preference of PFFs-injected mice receiving either saline or DCZ (DREADDs agonist) administration. **I-J**) Summarized graphs showing that PFFs-injected mice receiving saline injections exhibit impairment in their social novelty preference behavior of (I, saline-injected control, S1 = 198 [178, 220] sec, S2 = 275 [260, 338] sec, n = 5 mice, p = 0.008; saline-injected PFFs, S1 = 294 [244, 335] sec, S2 = 214 [168, 278] sec, n =5 mice, p = 0.09, MWU), which was rescued by DREADDs agonist DCZ injection (J, DCZ-injected controls, S1 = 180 [166, 213] sec, S2 = 294 [284, 347] sec, n = 5 mice, p = 0.008; DCZ-injected PFFs, S1 = 176 [134, 201] sec, S2 = 371 [280, 438] sec, n = 5 mice, p = 0.008, MWU).

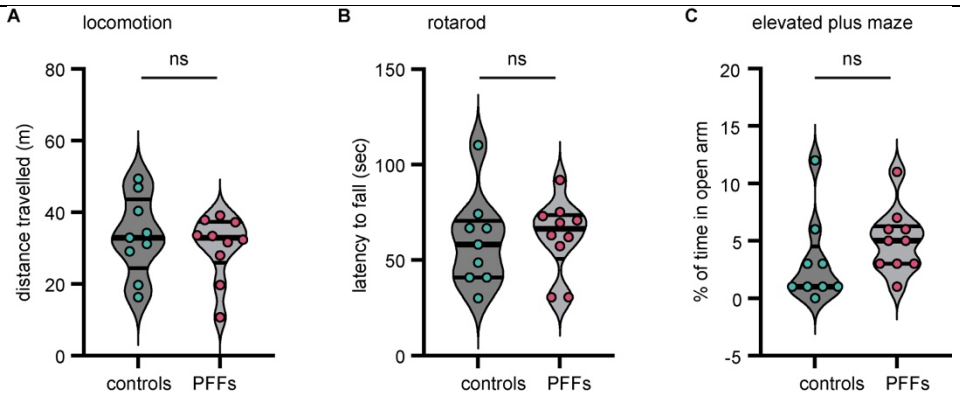

Supplementary Figure 1. PFFs-injected mice showed normal motor function and anxiety level at 3 mpi. A-C) Summarized graphs showing no difference between controls and PFFs-injected mice in the locomotion test (A, distance travelled, control = 33 [24, 44] m, n = 9 mice, PFFs = 33 [26, 37], n = 10 mice, p = 0.7, MWU), the rotarod test (B, latency to fall, control = 58 [41, 71] sec, n = 9 mice, PFFs = 66 [51, 74] sec, n = 10 mice, p = 0.5, MWU) and the elevated plus maze (C, % of time in open arm, control = 1 [1, 4.5]%, n= 9 mice, PFFs = 5 [3, 6]%, n = 10 mice, p = 0.08, MWU).

Of particular note, while the mPFC-BLA projections showed significant functional impairment in PFFs-injected mice, there was no significant loss of their presynaptic axonal terminals at 3 mpi. Given the critical role of mPFC inputs to the BLA in regulating social interaction, we sought to determine whether the deficient social novelty preference behavior could be rescued via activation of mPFC-BLA connections in PFFs-injected mice. To this end, we injected retrograde AAV-FlpO into the BLA and AAV-fDIO-hM3D(Gq)-mCherry into the mPFC (**Figure 5F**). This intersectional approach allows us to selectively stimulate mPFC-BLA synaptic neurotransmission using a chemogenetic approach. Three weeks after viral infections, PFFs-injected mice were subject to intraperitoneal injections of saline or deschlorozapine (DCZ) followed by social novelty preference behavior test. After saline injection, while controls showed normal social novelty preference, PFFs-injected mice were not able to distinguish novel-*versus* familiar-stimulus mice (i.e., S2 *vs* S1, **Figure 5H, I**), consistent with our data from previous cohort of animals (**Figure 5C, E**). In contrast, when PFFs-injected mice were subject to social

474 novelty preference test after DCZ injection, they showed strong preference to S2 *versus* S1

475 (**Figure 5J**), suggesting that their impaired social novelty preference has been rescued by

476 chemogenetic stimulation of mPFC-BLA connection.

477 Altogether, the above data suggest that the social novelty preference was disrupted by

478 α-Syn pathology in PFFs-injected mice at 3 mpi. Importantly, such disruption correlated with

479 impaired mPFC-BLA synaptic connection, which was then rescued by chemogenetic stimulation

480 of the mPFC-BLA connection in the PFFs-injected mice.

481

482 **Discussion**

483 In the present study, we performed longitudinal analyses of anatomical and physiological
484 changes associated with the formation of α-Syn aggregation, and provided novel insight into
485 how α-Syn aggregation impairs the connectivity and function of amygdala microcircuits. While
486 most research in the field has focused on the processes that initiate, facilitate, and/or
487 exacerbate α-Syn pathology formation and propagation, the present work highlights the less
488 explored, yet important, circuitry dysfunction associated with α-Syn aggregation that can
489 underlie some of the symptoms manifested by individuals afflicted by synucleinopathies. These
490 studies are of clinical relevance as strategies to prevent worsening of α-Syn pathology and to
491 repair the damaged circuits could make the current treatments for diseases like PD and DLB
492 more effective.

493

494 **Synaptic dysfunction occurs earlier than neurodegeneration in the BLA**

495 We demonstrated that α-Syn aggregation compromises synaptic function before structural
496 changes occur, including the loss of presynaptic axon terminal markers. In the context of our
497 recent work, even though functional deficits of cortico-BLA synapse may occur as early as 1 mpi
498 [34], loss of cortico-BLA presynaptic marker vGluT1 was only detected at the 6 mpi timepoint
499 (**Figure 2**). Moreover, BLA neurons are also prone to accumulating α-Syn aggregates, which
500 perhaps results in the loss of spines at 3 mpi (**Figure 4**) and their degeneration at much later
501 stages, i.e., 12 mpi. These observations are consistent with reports from the nigrostriatal system
502 in parkinsonian animals, showing deficits in dopamine release and degeneration of axons prior
503 to severe degeneration of dopaminergic neurons [4, 6, 17, 41, 42].

504 It is important to note that while BLA neurons exhibited loss of dendritic spines, the
505 initial release probability at cortico-BLA synapses increased at 3 and 6 mpi (**Figure 4**). This
506 observation is consistent with earlier findings from cultured hippocampal neurons, in which the
507 loss of postsynaptic spines and a paradoxical increase of presynaptic glutamate release were
508 reported [43]. Froula *et al* suggested that the enhanced presynaptic release probability might be
509 due to an increased size of readily releasable pool of neurotransmitters.
510
511 **Synaptic dysfunction is sufficient to drive the manifestation of behavioral phenotypes**
512 At the early stage of α-Syn based models, functional alterations of nigrostriatal pathway have
513 been reported to underlie the manifestation of parkinsonian motor deficits [4, 17, 44, 45]. In
514 the present study, we found that, prior to the loss of BLA neurons, mPFC-BLA synapses exhibited
515 functional impairment in PFFs-injected mice at 3 mpi, which temporally correlated with the
516 manifestation of defected social interaction behavior (**Figures 4 and 5**). Interestingly, the
517 impaired social novelty preference behavior was rescued by chemogenetic stimulation of the
518 defected mPFC-BLA pathway. Together, these findings support the hypothesis that synaptic
519 dysfunction is sufficient to drive the manifestation of behavioral phenotypes in
520 synucleinopathies. The intrastriatal PFFs-injected mice exhibited very specific deficits in emotion
521 related behavior. For example, while they exhibited deficits in social novelty preference (**Figure**
522 **5**) and social dominance behavior [31], no change in their anxiety levels in the elevated plus
523 maze test were detected [25, 31]. Though compelling evidence suggests that both social
524 behavior and anxiety are tightly regulated by the amygdala, it is plausible that performance in

525 the elevated plus maze test may involves distinct amygdala subcircuits from those activated
526 during the 3-chamber social interaction test [46, 47].
527
528 **Cell type-specific α-Syn expression and its implications in circuit dysfunction**
529 In a complex circuit, not all afferents within the same neurochemical category are
530 equally affected by α-Syn aggregation. For example, vGluT2$^+$ glutamatergic axons arising from
531 the thalamus are more resilient relative to vGluT1$^+$ axons in the BLA (**Figure 2**). This observation
532 is largely consistent with lower *Snca* mRNA levels in thalamic neurons as well as α-Syn
533 expression in their axon terminals [34, 48]. Moreover, evidence in the literature consistently
534 reports that Lewy body-like pS129$^+$ somatic aggregates are more abundant in cerebral cortical
535 regions relative to thalamic regions in intrastriatal PFFs models [3, 25, 26, 34, 49], suggesting
536 that the cerebral cortex and thalamus are affected differently by α-Syn pathology in diseased
537 state. Of relevance to the present work, it is known that cooperative activity and plasticity of
538 cortical and thalamic inputs are essential to normal amygdala function in the formation and
539 long-term storage of emotion memory [50, 51]. It remains to be determined how the disrupted
540 balance or cooperation of cortical and thalamic inputs to the BLA might impair emotion
541 encoding and regulation by the amygdala circuits. Remarkably, human imaging studies reported
542 that PD individuals diagnosed with depression showed a reduced activation of the amygdala in
543 the presence of aversive stimulations as well as a disconnected cortical (but not the thalamic)
544 inputs to the amygdala [27, 30]. Our findings of weakened cortical, but not thalamic inputs, to
545 the BLA might be of relevance to this clinical observation in PD individuals exhibiting
546 neuropsychiatric symptoms.

547 The complicated interaction and impact of α-Syn pathology on circuit function can also
548 partially explain why emotion dysregulation, including anxiety and depression, can occur at any
549 stages of the disease in PD or DLB individuals (e.g., even before the onset of motor symptoms),
550 which might vary depending on where the α-Syn pathology starts and how it can affect specific
551 circuits. While the present studies focus on the impact of α-Syn pathology on the amygdala
552 function and related behavior, we must acknowledge that degeneration of key neuromodulators
553 and their inputs to the amygdala (e.g., dopaminergic and noradrenergic systems) also play key
554 roles in the development of neuropsychiatric symptoms in PD and DLB.
555
556 **Conclusion**
557 We presented a combination of anatomical and physiological evidence to demonstrate a series
558 of circuitry events occurred in the amygdala circuits associated with α-Syn pathology in mouse
559 brain. Our findings not only support several well-accepted concepts in the field (e.g., synaptic
560 deficits prior to neurodegeneration), but also highlight the fact that we need to consider circuit
561 complexity before we can gain a thorough understanding on the contribution of α-Syn to brain
562 function in health and in diseased states.
563
564

565 **List of abbreviations**

566 BLA basolateral amygdala

567 α-Syn α-synuclein

568 PD Parkinson's disease

569 DLB Dementia with Lewy bodies

570 SNc Substantia nigra pars compacta

571 PFFs α-Syn preformed fibrils (PFFs).

572 EPSCs excitatory postsynaptic currents

573 mPFC medial prefrontal cortex

574 DREADDs designer receptors exclusively activated by designer drugs

575 IL-mPFC infralimbic subregion of mPFC

576 aCSF artificial cerebrospinal fluid

577 R_s series resistance

578 PFA paraformaldehyde

579 ANOVA analysis of variance

580 $pS129^+$ phospho-Ser129

581 LN Lewy neurite

582 LB Lewy body

583 mpi months-post-injection

584 vGluT1 vesicular glutamate transporter 1

585 vGluT2 vesicular glutamate transporter 2

586 SNCA Alpha Synuclein

587 DCZ deschloroclozapine

588

589

References cited:

1. Spillantini MG, Schmidt ML, Lee VMY, Trojanowski JQ, Jakes R, Goedert M: **α-Synuclein in Lewy bodies.** *Nature* 1997, **388:**839-840.
2. McCann H, Stevens CH, Cartwright H, Halliday GM: **α-Synucleinopathy phenotypes.** *Parkinsonism & Related Disorders* 2014, **20:**S62-S67.
3. Luk KC, Kehm V, Carroll J, Zhang B, O'Brien P, Trojanowski JQ, Lee VMY: **Pathological α-Synuclein Transmission Initiates Parkinson-like Neurodegeneration in Nontransgenic Mice.** *Science* 2012, **338:**949-953.
4. Janezic S, Threlfell S, Dodson PD, Dowie MJ, Taylor TN, Potgieter D, Parkkinen L, Senior SL, Anwar S, Ryan B, et al: **Deficits in dopaminergic transmission precede neuron loss and dysfunction in a new Parkinson model.** *Proceedings of the National Academy of Sciences* 2013, **110:**E4016-E4025.
5. Kim S, Kwon S-H, Kam T-I, Panicker N, Karuppagounder SS, Lee S, Lee JH, Kim WR, Kook M, Foss CA, et al: **Transneuronal Propagation of Pathologic α-Synuclein from the Gut to the Brain Models Parkinson's Disease.** *Neuron* 2019, **103:**627-641.e627.
6. Ledonne A, Cenere MM, Paldino E, D'Angelo V, D'Addario SL, Casadei N, Nobili A, Berretta N, Fusco FR, Ventura R, et al: **Morpho-Functional Changes of Nigral Dopamine Neurons in an α-Synuclein Model of Parkinson's Disease.** *Movement Disorders* 2023, **38:**256-266.
7. Lundblad M, Decressac M, Mattsson B, Björklund A: **Impaired neurotransmission caused by overexpression of α-synuclein in nigral dopamine neurons.** *Proceedings of the National Academy of Sciences of the United States of America* 2012, **109:**3213-3219.
8. Li J-Y, Englund E, Holton JL, Soulet D, Hagell P, Lees AJ, Lashley T, Quinn NP, Rehncrona S, Björklund A, et al: **Lewy bodies in grafted neurons in subjects with Parkinson's disease suggest host-to-graft disease propagation.** *Nat Med* 2008, **14:**501-503.
9. Desplats P, Lee H-J, Bae E-J, Patrick C, Rockenstein E, Crews L, Spencer B, Masliah E, Lee S-J: **Inclusion formation and neuronal cell death through neuron-to-neuron transmission of α-synuclein.** *Proceedings of the National Academy of Sciences* 2009, **106:**13010-13015.
10. Praschberger R, Kuenen S, Schoovaerts N, Kaempf N, Singh J, Janssens J, Swerts J, Nachman E, Calatayud C, Aerts S, et al: **Neuronal identity defines α-synuclein and tau toxicity.** *Neuron* 2023, **111:**1577-1590.e1511.
11. Mahul-Mellier A-L, Burtscher J, Maharjan N, Weerens L, Croisier M, Kuttler F, Leleu M, Knott GW, Lashuel HA: **The process of Lewy body formation, rather than simply α-synuclein fibrillization, is one of the major drivers of neurodegeneration.** *Proceedings of the National Academy of Sciences of the United States of America* 2020, **117:**4971-4982.
12. Kim YE, Lai TT, Kim YJ, Jeon B: **Preferential microglial activation associated with pathological alpha synuclein transmission.** *J Clin Neurosci* 2020, **81:**469-476.
13. Peng C, Gathagan RJ, Covell DJ, Medellin C, Stieber A, Robinson JL, Zhang B, Pitkin RM, Olufemi MF, Luk KC, et al: **Cellular milieu imparts distinct pathological α-synuclein strains in α-synucleinopathies.** *Nature* 2018, **557:**558-563.

632 14. Johnson ME, Stecher B, Labrie V, Brundin L, Brundin P: **Triggers, Facilitators, and**
633 **Aggravators: Redefining Parkinson's Disease Pathogenesis.** *Trends Neurosci* 2018, **42:**4-
634 13.
635 15. Fares MB, Jagannath S, Lashuel HA: **Reverse engineering Lewy bodies: how far have we**
636 **come and how far can we go?** *Nat Rev Neurosci* 2021, **22:**111-131.
637 16. Volpicelli-Daley Laura A, Luk Kelvin C, Patel Tapan P, Tanik Selcuk A, Riddle Dawn M,
638 Stieber A, Meaney David F, Trojanowski John Q, Lee Virginia MY: **Exogenous α-Synuclein**
639 **Fibrils Induce Lewy Body Pathology Leading to Synaptic Dysfunction and Neuron**
640 **Death.** *Neuron* 2011, **72:**57-71.
641 17. Tozzi A, Sciaccaluga M, Loffredo V, Megaro A, Ledonne A, Cardinale A, Federici M,
642 Bellingacci L, Paciotti S, Ferrari E, et al: **Dopamine-dependent early synaptic and motor**
643 **dysfunctions induced by alpha-synuclein in the nigrostriatal circuit.** *Brain* 2021,
644 **144:**3477-3491.
645 18. Ghiglieri V, Calabrese V, Calabresi P: **Alpha-Synuclein: From Early Synaptic Dysfunction**
646 **to Neurodegeneration.** *Front Neurol* 2018, **9:**295.
647 19. McGregor MM, Nelson AB: **Circuit Mechanisms of Parkinson's Disease.** *Neuron* 2019,
648 **101:**1042-1056.
649 20. Galvan A, Wichmann T: **Pathophysiology of parkinsonism.** *Clinical neurophysiology*
650 2008, **119:**1459-1474.
651 21. Sorrentino ZA, Goodwin MS, Riffe CJ, Dhillon J-KS, Xia Y, Gorion K-M, Vijayaraghavan N,
652 McFarland KN, Golbe LI, Yachnis AT, Giasson BI: **Unique α-synuclein pathology within**
653 **the amygdala in Lewy body dementia: implications for disease initiation and**
654 **progression.** *Acta Neuropathologica Commun* 2019, **7:**142.
655 22. Nelson PT, Abner EL, Patel E, Anderson S, Wilcock DM, Kryscio RJ, Eldik LJV, Jicha GA, Gal
656 Z, Nelson RS, et al: **The Amygdala as a Locus of Pathologic Misfolding in**
657 **Neurodegenerative Diseases.** *J Neuropathology Exp Neurology* 2017, **77:**2-20.
658 23. Flores-Cuadrado A, Ubeda-Bañon I, Saiz-Sanchez D, Martinez-Marcos A: **α-**
659 **Synucleinopathy in the Human Amygdala in Parkinson Disease: Differential**
660 **Vulnerability of Somatostatin- and Parvalbumin-Expressing Neurons.** *J Neuropathology*
661 *Exp Neurology* 2017, **76:**754-758.
662 24. Harding AJ, Stimson E, Henderson JM, Halliday GM: **Clinical correlates of selective**
663 **pathology in the amygdala of patients with Parkinson's disease.** *Brain J Neurology*
664 2002, **125:**2431-2445.
665 25. Burtscher J, Copin J-C, Rodrigues J, Kumar ST, Chiki A, Suduiraut M-IGd, Sandi C, Lashuel
666 HA: **Chronic corticosterone aggravates behavioural and neuronal symptomatology in a**
667 **mouse model of alpha-synuclein pathology.** *Neurobiol Aging* 2019, **83:**11-20.
668 26. Henderson MX, Cornblath EJ, Darwich A, Zhang B, Brown H, Gathagan RJ, Sandler RM,
669 Bassett DS, Trojanowski JQ, Lee VMY: **Spread of α-synuclein pathology through the**
670 **brain connectome is modulated by selective vulnerability and predicted by network**
671 **analysis.** *Nat Neurosci* 2019, **22:**1248-1257.
672 27. Hu X, Song X, Yuan Y, Li E, Liu J, Liu W, Liu Y: **Abnormal functional connectivity of the**
673 **amygdala is associated with depression in Parkinson's disease.** *Movement Disorders*
674 2015, **30:**238-244.

675 28. Thobois S, Prange S, Sgambato-Faure V, Tremblay L, Broussolle E: **Imaging the Etiology of**
676 **Apathy, Anxiety, and Depression in Parkinson's Disease: Implication for Treatment.**
677 *Curr Neurol Neurosci* 2017, **17:**76.
678 29. Bowers D, Miller K, Mikos A, Kirsch-Darrow L, Springer U, Fernandez H, Foote K, Okun M:
679 **Startling facts about emotion in Parkinson's disease: blunted reactivity to aversive**
680 **stimuli.** *Brain* 2006, **129:**3356-3365.
681 30. Yoshimura N, Kawamura M, Masaoka Y, Homma I: **The amygdala of patients with**
682 **Parkinson's disease is silent in response to fearful facial expressions.** *Neuroscience*
683 2005, **131:**523-534.
684 31. Stoyka LE, Arrant AE, Thrasher DR, Russell DL, Freire J, Mahoney CL, Narayanan A, Dib
685 AG, Standaert DG, Volpicelli-Daley LA: **Behavioral defects associated with amygdala and**
686 **cortical dysfunction in mice with seeded α-synuclein inclusions.** *Neurobiol Dis*
687 2019**:**104708.
688 32. Volpicelli-Daley LA, Luk KC, Lee VMY: **Addition of exogenous α-synuclein preformed**
689 **fibrils to primary neuronal cultures to seed recruitment of endogenous α-synuclein to**
690 **Lewy body and Lewy neurite–like aggregates.** *Nat Protoc* 2014, **9:**2135-2146.
691 33. West MJ: **Stereological methods for estimating the total number of neurons and**
692 **synapses: issues of precision and bias.** *Trends Neurosci* 1999, **22:**51-61.
693 34. Chen L, Nagaraja C, Daniels S, Fisk ZA, Dvorak R, Meyerdirk L, Steiner JA, Galvis MLE,
694 Henderson MX, Rousseaux MWC, et al: **Synaptic location is a determinant of the**
695 **detrimental effects of α-Synuclein pathology to glutamatergic transmission in the**
696 **basolateral amygdala.** *Elife* 2022, **11**.
697 35. Osterberg Valerie R, Spinelli Kateri J, Weston Leah J, Luk Kelvin C, Woltjer Randall L, Unni
698 Vivek K: **Progressive Aggregation of Alpha-Synuclein and Selective Degeneration of**
699 **Lewy Inclusion-Bearing Neurons in a Mouse Model of Parkinsonism.** *Cell Reports* 2015,
700 **10:**1252-1260.
701 36. Huang WC, Zucca A, Levy J, Page DT: **Social Behavior Is Modulated by Valence-Encoding**
702 **mPFC-Amygdala Sub-circuitry.** *Cell Rep* 2020, **32:**107899.
703 37. McGarry LM, Carter AG: **Prefrontal Cortex Drives Distinct Projection Neurons in the**
704 **Basolateral Amygdala.** *Cell Reports* 2017, **21:**1426-1433.
705 38. Likhtik E, Stujenske JM, Topiwala MA, Harris AZ, Gordon JA: **Prefrontal entrainment of**
706 **amygdala activity signals safety in learned fear and innate anxiety.** *Nat Neurosci* 2014,
707 **17:**106-113.
708 39. Xu S, Jiang M, Liu X, Sun Y, Yang L, Yang Q, Bai Z: **Neural Circuits for Social Interactions:**
709 **From Microcircuits to Input-Output Circuits.** *Front Neural Circuits* 2021, **15:**768294.
710 40. Felix-Ortiz AC, Tye KM: **Amygdala Inputs to the Ventral Hippocampus Bidirectionally**
711 **Modulate Social Behavior.** *J Neurosci* 2014, **34:**586-595.
712 41. Good CH, Hoffman AF, Hoffer BJ, Chefer VI, Shippenberg TS, Bäckman CM, Larsson N-G,
713 Olson L, Gellhaar S, Galter D, Lupica CR: **Impaired nigrostriatal function precedes**
714 **behavioral deficits in a genetic mitochondrial model of Parkinson's disease.** *Faseb J*
715 2011, **25:**1333-1344.
716 42. O'Keeffe GW, Sullivan AM: **Evidence for dopaminergic axonal degeneration as an early**
717 **pathological process in Parkinson's disease.** *Parkinsonism Relat Disord* 2018, **56:**9-15.

43. Froula JM, Henderson BW, Gonzalez JC, Vaden JH, McLean JW, Wu Y, Banumurthy G, Overstreet-Wadiche L, Herskowitz JH, Volpicelli-Daley LA: **α-Synuclein fibril-induced paradoxical structural and functional defects in hippocampal neurons.** *Acta Neuropathologica Commun* 2018, **6:**35.
44. Subramaniam M, Althof D, Gispert S, Schwenk J, Auburger G, Kulik A, Fakler B, Roeper J: **Mutant α-Synuclein Enhances Firing Frequencies in Dopamine Substantia Nigra Neurons by Oxidative Impairment of A-Type Potassium Channels.** *J Neurosci* 2014, **34:**13586-13599.
45. Guatteo E, Rizzo FR, Federici M, Cordella A, Ledonne A, Latini L, Nobili A, Viscomi MT, Biamonte F, Landrock KK, et al: **Functional alterations of the dopaminergic and glutamatergic systems in spontaneous α-synuclein overexpressing rats.** *Exp Neurol* 2017, **287:**21-33.
46. Bian WJ, Brewer CL, Kauer JA, de Lecea L: **Adolescent sleep shapes social novelty preference in mice.** *Nat Neurosci* 2022, **25:**912-923.
47. Gonzalez LE, Andrews N, File SE: **5-HT1A and benzodiazepine receptors in the basolateral amygdala modulate anxiety in the social interaction test, but not in the elevated plus-maze.** *Brain Res* 1996, **732:**145-153.
48. Geertsma HM, Fisk ZA, Sauline L, Prigent A, Kurgat K, Callaghan SM, a S-PDC, Henderson MX, Rousseaux MWC: **A topographical atlas of alpha-synuclein dosage and cell type-specific expression in adult mouse brain and peripheral organs.** *NPJ Parkinsons Dis* 2024, **10:**65.
49. Chatterjee D, Sanchez DS, Quansah E, Rey NL, George S, Becker K, Madaj Z, Steiner JA, Ma J, Galvis MLE, et al: **Loss of One Engrailed1 Allele Enhances Induced α-Synucleinopathy.** *J Park Dis* 2019, **9:**315-326.
50. Shin R-M, Tully K, Li Y, Cho J-H, Higuchi M, Suhara T, Bolshakov VY: **Hierarchical order of coexisting pre- and postsynaptic forms of long-term potentiation at synapses in amygdala.** *Proceedings of the National Academy of Sciences* 2010, **107:**19073-19078.
51. Siguròsson T, Sigurdsson T, Cain CK, Doyère V, LeDoux JE: **Asymmetries in long-term and short-term plasticity at thalamic and cortical inputs to the amygdala in vivo.** *Eur J Neurosci* 2010, **31:**250-262.